

The Very Highly Ionized Broad Absorption Line System of the QSO SBS1542+541

Randal C. Telfer, Gerard A. Kriss, Wei Zheng, and Arthur F. Davidsen
Center for Astrophysical Sciences, Johns Hopkins University, Baltimore, MD, 21218-2686;
rt19@pha.jhu.edu, gak@pha.jhu.edu, zheng@pha.jhu.edu, afd@pha.jhu.edu

and

Richard F. Green
Kitt Peak National Observatory, National Optical Astronomy Observatories, P.O. Box 26732,
950 North Cherry Ave., Tucson, AZ, 85726-6732

ABSTRACT

We have analyzed the broad absorption line system of the bright ($V \sim 16.5$) high-redshift ($z = 2.361$) QSO SBS1542+541 using UV spectra from the HST FOS along with optical data from the MMT and the Steward Observatory 2.3m telescope. These spectra offer continuous wavelength coverage from 1200 to 8000 Å, corresponding to $\sim 340 - 2480$ Å in the QSO rest frame. The line of sight to the object contains only three identified intervening Lyman-limit absorption systems. Only one of these is optically thick at the Lyman edge, a low-redshift ($z = 0.156$) system with a strong Lyman edge observed at 1055 Å (314 Å in the rest frame) in a Hopkins Ultraviolet Telescope spectrum from the Astro-2 mission. The spectra therefore offer a rare opportunity to study broad absorption lines in the rest-frame extreme UV.

We find that the broad absorption line system is lacking in species of relatively low ionization often seen in broad absorption systems, such as C III, O III, and Si IV. Instead, the system is dominated by very high-ionization species. The strongest features correspond to O VI, Ne VIII, and Si XII. In addition to other high-ionization lines, we identify apparently saturated broad Lyman-series lines of order Ly γ and higher.

There is strong evidence for partial occultation of the QSO emission source, particularly from the higher-order Lyman lines which indicate a covered fraction less than 0.2. With the exception of C IV and N V, which are low-ionization species in the context of this system, all of the other lines depress the flux by more than 20%. Absorption from Ly α also depresses the flux more than 20%, indicating that there are at least two different regions contributing to H I absorption. Overall, the data suggest a correlation between a larger covered fraction and a higher state of ionization. These observations reveal inhomogeneity in the ionization structure of the broad absorption line gas.

We have used photoionization models to constrain the total column density and ionization state of the system. A single-slab model consistent with our observational

limits on the column densities requires $N_H \approx 5 \times 10^{22} \text{ cm}^{-2}$ and an incident ionization parameter $U \approx 2$. Since the observed covered fractions suggest multiple zones, we also produced a two-slab model and find $10^{21} \text{ cm}^{-2} < N_H < 10^{23} \text{ cm}^{-2}$ and $0.08 < U < 4$ for the smaller zone, and $N_H \gtrsim 3 \times 10^{21} \text{ cm}^{-2}$ and $U \gtrsim 2$ for the larger zone. We suggest that the different covered fractions can be explained by either a special line of sight through a disk-like geometry or by the existence of density fluctuations of a factor $\gtrsim 2$ in the BAL gas. The large column density and high state of ionization suggest that the system is likely associated with an X-ray “warm absorber”.

1. INTRODUCTION

Observations of SBS1542+541 using the International Ultraviolet Explorer (Porter *et al.* unpublished¹) show that there is significant continuum flux down to below 1200 Å, corresponding to ~ 360 Å in the rest frame. This made the object a good candidate for possibly observing He II Ly α $\lambda 304$ absorption in the intergalactic medium with the Hopkins Ultraviolet Telescope (HUT) during the Astro-2 mission. Observations of HS1700+64 ($z = 2.743$) on the same mission successfully measured the He II opacity (Davidsen, Kriss, & Zheng 1996). However, during the observations of SBS1542+541 on 1995 March 16 we discovered that there was a cutoff in flux slightly redshifted from the expected position of the He II Ly α absorption, causing us to suspect that the observed feature was a Lyman limit from a low-redshift intervening absorber. To further investigate this possibility we performed observations on 1995 September 3 with the G130H, G190H, and G270H gratings of the HST FOS. The presence of the intervening system is verified by a strong Mg II $\lambda\lambda 2796, 2804$ doublet in the G270H spectrum at the same redshift ($z = 0.156$) as the Lyman edge visible in the HUT spectrum. Fortuitously, the FOS spectra also reveal broad absorption lines from several very highly-ionized species, many of which have never before been observed in a broad absorption line QSO. It is the study of this broad absorption system that is the focus of our present interest.

Roughly 10% of radio-quiet QSOs exhibit broad ($\gtrsim 2000 \text{ km s}^{-1}$) blueshifted absorption features associated with the QSO, known as broad absorption lines (BALs), with outflow velocities generally $0 - 0.1c$ (Turnshek 1984). These objects are collectively referred to as broad absorption line QSOs, or BALQSOs. The absorption features most commonly observed are Ly α $\lambda 1216$, C IV $\lambda 1549$, Si IV $\lambda 1397$, and N V $\lambda 1240$, though low-ionization lines, usually Mg II $\lambda 2798$ and Al III $\lambda 1857$, are observed in some objects, usually called low-ionization BALQSOs. Higher-ionization lines are sometimes reported, up through Ne VIII $\lambda 774$ and Mg X $\lambda 615$ (Korista & Arav 1997).

When studying a BAL system, one of the primary goals is to determine column densities of

¹The research was submitted in 1991 for publication in *ApJ*, but the work was never fully completed due to the illness of Alain C. Porter that led to his untimely death in 1993.

the various observed ions, which are used in turn to derive the ionization state of the gas and its chemical composition. To determine column densities, it is necessary to measure the optical depth of the absorption as a function of outflow velocity. In deriving the optical depth from the relative depression of the continuum flux, one typically makes the assumptions that (1) there are no unresolved narrow lines in the BAL troughs, (2) scattered radiation does not fill in the absorption troughs, and (3) the BAL gas completely and homogeneously covers the continuum source on the observed line of sight. If any of these assumptions are invalid, then the true column densities could be much greater than those inferred from the observations. Based on high-resolution observations of BAL troughs (Barlow & Junkkarinen 1994), assumption (1) appears to be a good one. Studies of BAL geometry (Turnshek 1988; Hamann, Korista, & Morris 1993) suggest that the global BAL region covering factor, which is the fractional solid angle subtended by the BAL gas as seen from the continuum source, is generally $\lesssim 0.2$ (except possibly in low-ionization BALQSOs; Boroson & Meyers 1992; Turnshek *et al.* 1997). If the global BAL covering factor is small, and especially if the outflow velocities are large, then (2) should be adequately satisfied, although spectropolarimetry suggests that some scattered light is present in the depths of the BAL troughs (Goodrich & Miller 1995; Cohen *et al.* 1995). However, there is evidence that assumption (3) is invalid: in some instances absorption doublets appear to show saturation of the components but not at zero intensity (Korista *et al.* 1992), implying that the absorbing gas only partially covers the source. More definite evidence for partial covering has been observed in the so-called associated or $z_{abs} \approx z_{em}$ absorption lines (Hamann *et al.* 1997; Hamann, Barlow, & Junkkarinen 1997), which are distinguished from BALs primarily by being much narrower, usually having widths \lesssim a few hundred km s^{-1} . The fraction of the continuum source occulted by the BAL region along the line of sight is called the covered fraction, or for clarity the *continuum source covered fraction*, to distinguish it from the global BAL region covering factor. For the remainder of this paper, we will use the term *covered fraction* to refer to the continuum source covered fraction.

We begin with a presentation of the observations used for this research (§2), followed by a discussion of the spectra and how we fit the BALs in order to estimate minimum column densities and covered fractions of the absorbing ions (§3). We then discuss some properties of the system that can be inferred in the context of a photoionization model, including constraints on the ionization state and column density and the resulting implications for the geometry and physical structure of the gas (§4). Finally we summarize the characteristics of this particular BALQSO that make it so interesting and potentially relevant to the study of BALQSOs as a whole (§5).

2. OBSERVATIONS

Our observations with the HST FOS were performed on 1995 September 3. They include 14880 s with the G130H grating, 5470 s with G190H, and 1600 s with G270H. These three spectra are shown in Figure 1. The G130H data had to be corrected for a flickering diode not recognized by the FOS pipeline at the time of processing. This diode (#22 affecting wavelengths

1162 – 1167 Å) was added to the list of dead diodes and the spectrum was reprocessed. These spectra have a resolution of 1 Å (G130H), 1.44 Å (G190H), and 2 Å (G270H), corresponding to a range of velocity resolution of 183 – 287 km s⁻¹ for the FOS data.

At optical wavelengths we use two observations. The first was performed on 1995 April 1 with the MMT and covers 3120 – 4770 Å with a resolution of 3.2 Å, corresponding to a velocity resolution 200 – 307 km s⁻¹. The other observation was performed on 1995 June 3 with the Steward Observatory 2.3m telescope, including the wavelength range 4640 – 8010 Å with a 5.54 Å resolution, corresponding to a velocity resolution of 207 – 358 km s⁻¹. The MMT spectrum is of excellent quality in the wavelength region below 3500 Å for a ground-based observation, which is fortunate since this reveals well the broad O VI absorption feature centered at ~ 3350 Å. The optical spectra are shown in Figure 2.

Together, these five spectra provide us with continuous wavelength coverage from 1200 to 8000 Å, or $\sim 340 - 2480$ Å in the QSO rest frame. For the purpose of identifying the $z = 0.156$ intervening absorption system, we also refer to the HUT spectrum of SBS1542+541 obtained on 1995 March 16 during the Astro-2 mission, shown in Figure 3. A normalized template created from blank-field spectra was used to remove airglow. This removes the broad wings of Ly α , but some narrow residuals remain for Ly α and a few other strong lines which were removed by hand. The spectrum is of low S/N due to the short integration time (4320 s), so we do not use it for the analysis of the BAL system.

We have also analyzed X-ray data from a 5632 s exposure of SBS1542+541 obtained with the *ROSAT* Position Sensitive Proportional Counter (PSPC) on 1993 August 14. The observed count rate was 7.02×10^{-3} count s⁻¹. The S/N is too low to derive meaningful information about the spectral shape, so we use the data only to estimate the X-ray flux. This is discussed further in §4.1.

3. ANALYSIS

3.1. General Comments

We corrected the spectra for Galactic extinction based on a column density of neutral hydrogen along the line of sight of $N(H) = 1.30 \times 10^{20}$ cm⁻² (Stark *et al.* 1992). Using a conversion of $E_{(B-V)} = N(H)/5.2 \times 10^{21}$ cm⁻² (Shull & Van Steenberg 1985), this corresponds to an extinction $E_{(B-V)} = 0.025$. We then performed the extinction correction using the formulation of Cardelli, Clayton, & Mathis (1989), assuming $R_V = 3.1$.

In order to estimate the errors in the optical data, we fit small bands of apparently featureless continuum in each spectrum. Near the C IV $\lambda\lambda 1548, 1551$ feature in the Steward data, we fit the region 4840 – 4955 Å. We find that the error per pixel is around 2.8×10^{-17} erg cm⁻² s⁻¹ Å⁻¹, corresponding to a S/N per pixel of ~ 30 . We used this value to produce a constant error array

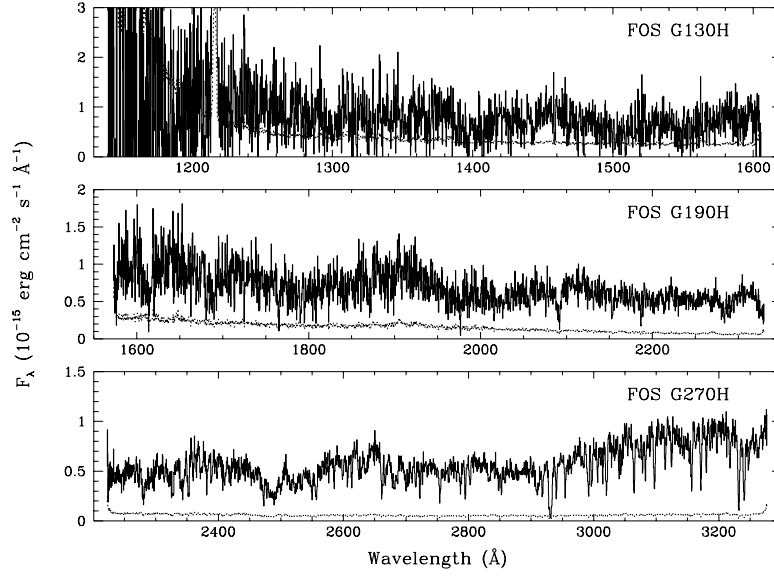


Fig. 1.— HST FOS spectra of SBS1542+541 (solid lines) along with the 1σ errors per pixel (dotted lines).

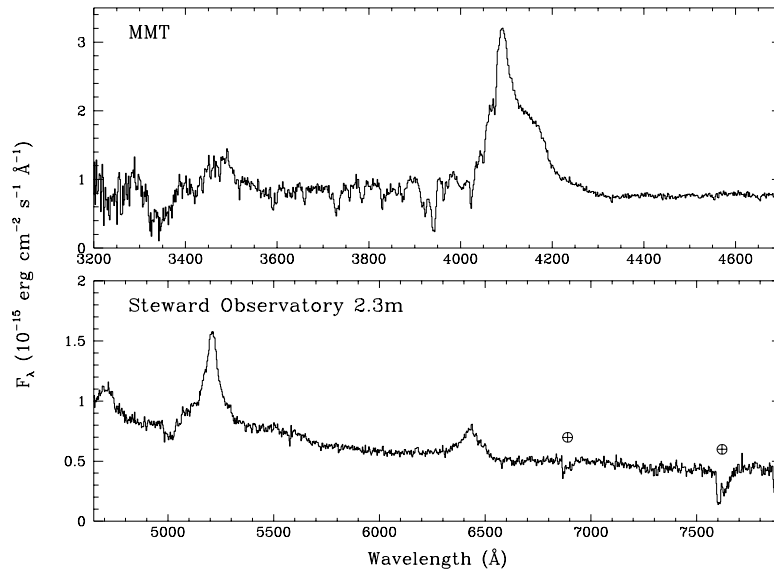


Fig. 2.— Optical spectra of SBS1542+541 from the MMT and Steward Observatory 2.3m telescope.

that was used in the fit of C IV. In the MMT spectrum, we fit $3667 - 3707 \text{ \AA}$ and found an error per pixel of $4.5 \times 10^{-17} \text{ erg cm}^{-2} \text{ s}^{-1} \text{ \AA}^{-1}$, corresponding to a S/N per pixel of ~ 20 . Again we simply produced a constant error array that was used in the fit of Ly α , N V $\lambda\lambda 1239, 1243$, and O VI $\lambda\lambda 1032, 1038$. However, given that the observation includes short wavelengths so near the atmospheric limit, the S/N is lower at the shorter wavelengths. Hence, we realize that this is probably an overestimate of the errors in the region of Ly α and N V and an underestimate of the errors near O VI, but since there are no spectral regions near these lines that can be well fit to estimate the errors, we will use this constant value.

Many of the problems associated with studying BALs are minimized in the spectrum of SBS1542+541. Due to the relatively small velocity width of the lines as well as the apparent lack of low-ionization species, most of the interesting lines are not blended and therefore the continuum is generally well-defined in the vicinity of the broad absorption features. Also, the line of sight to the object contains an unusual paucity of intervening Lyman-limit absorption systems. We identify only three at $z = 2.246$, $z = 0.721$, and $z = 0.156$. In the next section we briefly discuss each narrow-line system. A more comprehensive study of the intervening narrow-line systems (*e.g.* Vogel & Reimers 1995) would require data of higher S/N.

3.1.1. Intervening Narrow-Line Systems

The $z = 2.246$ system is clearly established by definite Lyman-series lines through Ly ϵ as well as lines from Ly6 – 8 that appear to be blended with other narrow lines, presumably from the Ly α forest. In addition, there are strong lines corresponding to C III $\lambda 977$ and C II $\lambda 903$ along with possible lines from O IV $\lambda 788$ and O III $\lambda 833$. This system overlaps the broad absorption in velocity space, precluding an accurate estimate of the column density from the Lyman-edge opacity, since the relative contribution of each system to the flux depression around 2950 \AA is not known. However, given that we find in §3.5 that most of the neutral hydrogen from the BAL system covers only $\sim 20\%$ of the continuum source, we can conclude that at least some of this flux depression must be due to the Lyman limit of the $z = 2.246$ system, since the full depression is $\sim 40\%$ of the total continuum flux. This enables us to estimate that the total column of neutral hydrogen in this system probably lies in the range $\log N(H) \approx 16.65 - 16.90$. The system could be intrinsic rather than intervening; however, given that the observed metal lines suggest a lower ionization level than the broad lines, we assume in our analysis that it is physically distinct from the highly-ionized BAL system.

The system at $z = 0.721$ is identified mainly on the basis of the very strong lines of Ly α ($W_\lambda \approx 2.8 \text{ \AA}$) and Ly β ($W_\lambda \approx 1.8 \text{ \AA}$) that have unusually broad profiles, the Ly α line having a Full Width at Zero Absorption (FWZA) $\approx 900 \text{ km s}^{-1}$ and Ly β having a FWZA $\approx 750 \text{ km s}^{-1}$. A weak Ly γ feature can be seen, as well as a possible feature from C III $\lambda 977$ blended with the broad absorption of Si XII $\lambda 521$. It is difficult to confirm the presence of any Lyman-limit feature, which should lie at 1569 \AA , due to the uncertain continuum shape in this region. There does appear to

be some small decrease in the flux, but the situation is complicated by the fact that QSOs can only rarely be observed so far into the rest-frame UV, and consequently knowledge of the broad emission line properties in this region is extremely limited. We estimate $\log N(H) \lesssim 16.8$.

The redshift of the $z = 0.156$ system is calculated from the strong Mg II $\lambda\lambda 2796, 2804$ doublet that occurs around 3235 \AA . Absorption from Ly α and possibly C IV $\lambda\lambda 1548, 1551$ are also detected. None of the higher-order Lyman lines can be seen since they lie below the wavelength coverage of our data. However, the system is firmly established by the Mg II doublet and by the presence of the strong Lyman-limit feature at $\sim 1055 \text{ \AA}$ visible in the HUT spectrum of this object (Figure 3).

3.2. Broad Absorption Lines

We have identified broad absorption features corresponding to resonance lines of H I, C IV, N V, O VI, Ne V through Ne VIII, Mg X, Si XII, and Ar VII. Each feature is primarily characterized by a single trough that is blue-shifted at line center by $\sim 11000 - 12000 \text{ km s}^{-1}$ with respect to the rest frame and has a width of $2000 - 3000 \text{ km s}^{-1}$. The troughs are fairly flat across the bottom with no obvious consistent structure and have sharp velocity cutoffs on both the red and blue end. Because of the high ionization levels and small widths of the lines, many of the doublets are resolved in velocity space, including Ne VIII $\lambda\lambda 770, 780$, Mg X $\lambda\lambda 610, 625$, and Si XII $\lambda\lambda 499, 521$. The Lyman-series lines through Ly ϵ are also resolved, with the exception of Ly β which is strongly blended with O VI $\lambda\lambda 1032, 1038$.

There are several other possible lines that are either part of a strong blend or occur in portions of the spectrum where the continuum level is not well-defined and hence the existence of the line is difficult to determine:

1. Absorption from O IV $\lambda 788$ could be present around 2550 \AA , but the continuum shape is uncertain due to the Ne VIII broad emission line and a blend of narrow absorption lines.
2. There appears to be some slight evidence for an O V $\lambda 630$ feature around 2035 \AA , but the absorption is either weak or the covered fraction is small ($\lesssim 0.2$). Also, this lies in between the apparent O V broad emission line and the Mg X $\lambda 625$ BAL, again making the continuum shape uncertain.
3. There is a dip in the flux shortward of an apparent broad emission line around 1900 \AA , possibly Ne VI $\lambda 559 +$ Ne V $\lambda 568$. The dip extends from $\sim 1670 \text{ \AA}$ to $\sim 1830 \text{ \AA}$ and could be a blend of several possible BALs including O IV $\lambda\lambda 553, 554$, Ne V $\lambda 568$, Ne VI $\lambda 559$, and Al XI $\lambda\lambda 550, 568$.

For the reasons stated above and the uncertainties in the profiles, we make no attempt to fit or deblend any of the above lines. We did measure the equivalent width of the broad feature around

1400 Å since this feature appears to be well-defined. This is likely a blend of Ne VI λ 433, Mg VIII λ 430, and possibly Mg VII λ 429. Table 1 lists atomic data for all of the resonance lines relevant to this paper.

Although the absorption system of SBS1542+541 qualifies it as a BALQSO according to the canonical definition of the class (Weymann, Carswell, & Smith 1981), it certainly has characteristics that distinguish it from “classical” BALQSOs. The line widths of 2000 – 3000 km s⁻¹ are relatively small—absorption over a range of velocities exceeding 10000 km s⁻¹ is common in BALQSOs. In addition, the features from C IV, N V, and Ly α are quite weak relative to “classical” systems, and absorption from Si IV λ λ 1394, 1403, a feature that is virtually omnipresent in BAL systems, is absent completely. Thus objects such as SBS1542+541 would be excluded from typical searches for BALQSOs which look for these features to be strong. We also find no evidence for absorption by other commonly observed low-ionization species such as C III, N III, N IV, and O III. Absorption from P V λ λ 1118, 1128, sometimes reported in broad absorption, is also not observed. There is a feature with the right profile shape and at the right wavelength to be Fe III λ 1123, but the feature is weak and the existence of Fe III would require a state of ionization much lower than that inferred from the other lines (§4.1), so we dismiss the feature as a probable cluster of Ly α -forest lines. The absence of low-ionization species, particularly Si IV, is useful for constraining the ionization state of the gas (§4).

In Figure 4 we show for reference a combined spectrum of the FOS and optical data, corrected for Galactic extinction and rebinned for higher S/N. All of the identified broad absorption features are labeled, as are the prominent broad emission lines and several intervening absorption features.

3.3. Broad Line Fits

For fitting purposes we attempted to develop optical depth templates from various observed absorption profiles such as C IV λ λ 1548, 1551 and Ne VIII λ λ 770, 780 (see Korista *et al.* 1992). However, we found that no single derived optical depth template was able to fit all of the observed lines satisfactorily, due mainly to slight variations in the widths of the profiles. Instead of a rigid template, it is necessary to use a more flexible absorption profile. We use two such profiles, one a simple Gaussian and the other a profile that we will refer to as the “flat profile”, an absorption profile that we synthesized in order to match the primary characteristics of the observed troughs, specifically the relatively flat bottoms and sharp velocity cutoffs. The flat profile is a feature of constant optical depth smoothed at each edge by a semi-Gaussian with FWHM fixed at the instrumental resolution. Each of these profiles provides a simple way to characterize the absorption features by three free parameters: the velocity centroid, the FWHM, and the equivalent width.

Table 2 shows the resulting fit parameters for the flat template, and Table 3 shows the parameters for the Gaussian fits. All of the fits were performed with the IRAF task *specfit* (Kris 1994). We fit a separate profile to each doublet component, even when the components are

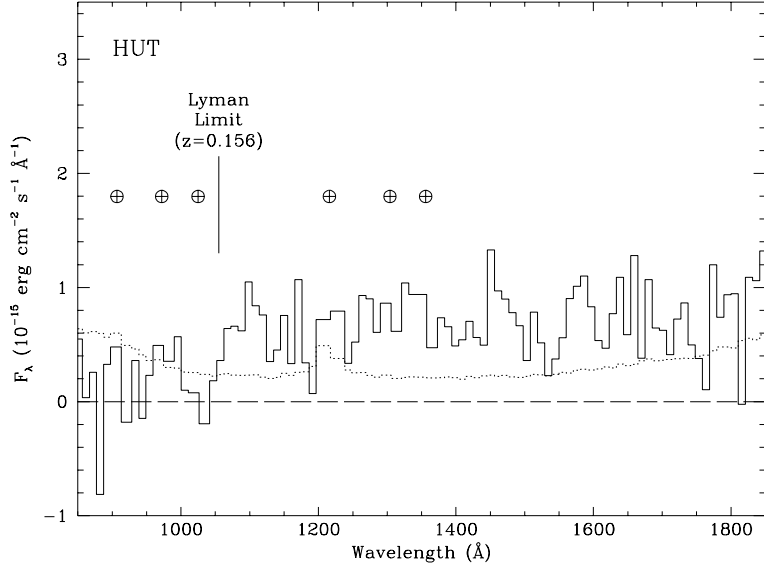


Fig. 3.— HUT spectrum of SBS1542+541 (solid line) after airglow subtraction, rebinned by 10 Å, along with 1σ errors per bin (dotted line). The \oplus symbols indicate where pixels were removed to eliminate the residual airglow from the strongest lines that remained after airglow subtraction using a blank-field template. The location of the Lyman-limit feature from the $z = 0.156$ intervening system is marked.

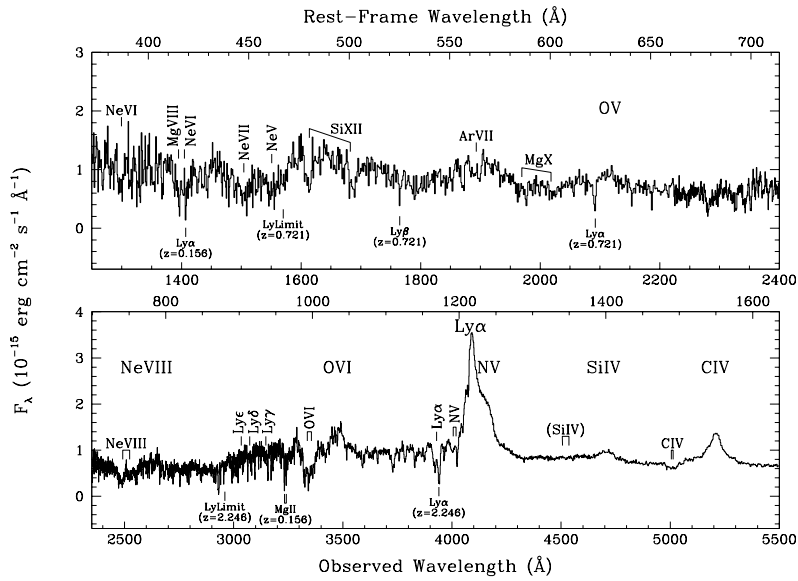


Fig. 4.— Combined spectra, extinction-corrected and rebinned for higher S/N. The broad absorption lines and prominent broad emission lines are labeled above the spectrum, some intervening absorption features below.

Table 1. Atomic Data^a

Ion	Creation IP(eV)	Destruction IP(eV)	$\lambda(\text{\AA})$	Oscillator Strength
H I	0.0	13.6	1215.67	0.416
			1025.72	0.0790
			972.54	0.0290
			949.74	0.0139
			937.80	0.00780
C IV	47.9	64.5	1548.20	0.190
			1550.77	0.0952
N V	77.5	97.9	1238.82	0.157
			1242.80	0.0780
O V	77.4	113.9	629.73	0.515
O VI	113.9	138.1	1031.93	0.133
			1037.62	0.0661
			1037.62	0.0661
Ne V	97.1	126.2	480.41	0.110
			568.42	0.0928
Ne VI	126.2	157.9	399.82	0.0844
			401.14	0.168
			433.18	0.0505
			558.59	0.0907
Ne VII	157.9	207.3	465.22	0.389
Ne VIII	207.3	239.1	770.41	0.103
			780.32	0.0505
Mg VII	186.5	225.0	429.13	0.0801
Mg VIII	225.0	266.0	430.47	0.0763
Mg X	328.2	367.5	609.79	0.0842
			624.95	0.0410
Al XI	399.4	442.1	550.03	0.0773
			568.15	0.0375
Si IV	33.5	45.1	1393.76	0.524
			1402.77	0.260
Si XII	476.1	523.5	499.40	0.0719
			520.67	0.0345
Ar VII	91.0	124.3	585.75	1.24

^aFrom Verner, Barthel, & Tytler (1994)

strongly blended as is the case for C IV and N V. We constrained the velocity centroids and widths of the individual components of the multiplet to be the same during the fits. Whenever two lines are blended, the equivalent width of the entire blend is given. The quoted errors on all quantities are purely 1σ confidence limits derived from the error matrix of the fit.

Only the most obvious narrow lines (FWHM \sim instrumental resolution, significance $\gtrsim 3\sigma$) were deblended from the broad lines, with all other features in the wavelength range of the BALs being treated as part of the BAL profiles. Less-significant narrow lines were sometimes fit outside the BAL profiles to improve the continuum fit. The presence of other narrow lines in the BAL profiles could cause additional uncertainty in the fit parameters. This is particularly true for Ly α , N V, O VI, and Ly γ through Ly ϵ , which lie in the portion of the spectrum where the Ly α forest is most dense. The fits for Si XII and to a lesser extent Mg X show some deviation from the observed profiles (see Figure 5) indicating that these also are probably somewhat corrupted by narrow lines. The possible effects of blending on the derived column densities and covered fractions are discussed in §3.4 and §3.5, respectively. For the fit of O VI, the Ly β BAL corresponding to the best fit of the higher-order Lyman lines, including a partial covered fraction as discussed in §3.5, was also deblended from the absorption profile. If there is additional Ly β corresponding to the stronger Ly α line, we could still be overestimating the strength of O VI.

Both profiles are capable of producing reasonable fits to the data, which is why we fit every feature with each profile. Because we created the flat profile specifically to fit the shapes of the observed absorption features, it achieves more satisfying fits than the Gaussian by eye, but only slightly better in χ^2 because of the generally low S/N. The tails of the Gaussians extend out slightly beyond where there is any apparent absorption, causing the equivalent widths of the Gaussian fits to be generally somewhat larger than those of the flat profile. Because the flat profile provides better fits, we believe that it parameterizes better the basic characteristics of the lines. However, using both profiles helps to characterize the uncertainties of our results associated with the uncertainty of the profile shape.

3.4. Minimum Column Densities

As we discuss in §3.5, we believe that the covered fractions of the different absorbing ions are significantly less than unity, and that the absorption may in many cases be optically thick. Without knowing the covered fraction, it is not possible to determine accurately the optical depth of the lines, and hence to determine the column densities. We can, however, put a good lower limit on the absorbing columns by calculating the column densities under the assumption of a covered fraction of unity. Rather than estimate the columns from the linear portion of the curve of growth, we derive values from direct integration of the optical depth of the best-fit absorption profiles. We produce the best fit possible for the lines from each ion assuming a covered fraction of unity, with the constraint that the ratio of the optical depths of the individual components is fixed by the oscillator strengths. To facilitate this, for the Gaussian fits we use a Gaussian defined in terms

Table 2. Fit Parameters: Flat Profile

Ion	$\lambda(\text{\AA})$	centroid(km s ⁻¹)	FWHM(km s ⁻¹)	$W_\lambda(\text{\AA})$
H I	1215.67	-11480 ± 30	2860 ± 70	10.24 ± 0.65
	972.54	-11120 ± 20	1940 ± 50	3.68 ± 0.30
	949.74			3.08 ± 0.31
	937.80			3.78 ± 0.30
C IV	1548.20, 1550.77	-11400 ± 70	3190 ± 190	7.95 ± 0.80
N V	1238.82, 1242.80	-11370 ± 50	27400 ± 100	5.34 ± 0.51
O VI	1031.93, 1037.62	-11340 ± 30	3260 ± 70	33.5 ± 1.6
Ne V	480.41	-11810 ± 70	2970 ± 150	4.84 ± 0.79
Ne VI	399.82, 401.14	-10410 ± 50	2530 ± 120	5.97 ± 0.80
Ne VII	465.22	-11350 ± 80	3150 ± 180	6.00 ± 0.88
	770.41	-11360 ± 20	2730 ± 40	10.07 ± 0.51
Ne VIII	780.32			6.05 ± 0.37
	609.79	-11750 ± 50	3110 ± 110	4.50 ± 0.82
Mg X	624.95			3.91 ± 0.70
	499.40	-11570 ± 60	3160 ± 130	5.64 ± 0.76
Si XII	520.67			5.86 ± 0.67
	585.75	-11540 ± 60	2910 ± 130	4.34 ± 0.73
Ar VII				
Ne VI+Mg VIII	433.18, 430.47	11.2 ± 1.1

Table 3. Fit Parameters: Gaussian

Ion	$\lambda(\text{\AA})$	centroid(km s ⁻¹)	FWHM(km s ⁻¹)	$W_\lambda(\text{\AA})$
H I	1215.67	-11290 ± 90	2150 ± 100	9.95 ± 0.60
	972.54	-11360 ± 50	1480 ± 100	3.42 ± 0.30
	949.74			2.81 ± 0.29
	937.80			3.02 ± 0.29
C IV	1548.20, 1550.77	-11330 ± 100	3110 ± 330	10.8 ± 1.8
N V	1238.82, 1242.80	-11570 ± 190	2160 ± 200	7.70 ± 0.50
O VI	1031.93, 1037.62	-11090 ± 160	3010 ± 230	29.9 ± 3.2
Ne V	480.41	-11950 ± 280	2850 ± 610	5.6 ± 1.1
Ne VI ^a	399.82, 401.14
Ne VII	465.22	-11530 ± 240	2830 ± 620	7.0 ± 1.3
Ne VIII	770.41	-11630 ± 80	2530 ± 180	12.24 ± 0.57
	780.32			7.33 ± 0.52
Mg X	609.79	-11670 ± 220	3050 ± 540	5.1 ± 1.3
	624.95			4.7 ± 1.1
Si XII	499.40	-11200 ± 580	2730 ± 270	6.5 ± 1.1
	520.67			7.46 ± 0.64
Ar VII	585.75	-11500 ± 280	2760 ± 410	5.31 ± 0.67
Ne VI+Mg VIII	433.18, 430.47	14.5 ± 3.2

^aParameters for the Ne VI feature are not listed because no minimum in χ^2 could be achieved that provided a good fit to the data

of optical depth rather than flux. The column densities with statistical errors as calculated from these fits are shown in Table 4. Since none of the lines are optically thick under the assumption of total covering, the uncertainty in the measured column densities due to the possible existence of narrow-line blends in the BALs should be relatively small.

Some of the ions, particularly Mg X, Si XII, and H I, exhibit multiple lines with similar apparent optical depths despite different oscillator strengths, suggesting that the lines are likely saturated and therefore that the continuum source is not fully occulted by the absorber. As a result, the fits to these features under the assumption of a covered fraction of unity are poor, particularly for the higher-order Lyman lines, for which no reasonable fit could be achieved. Also, none of the BAL troughs depress the flux more than $\sim 60\%$, consistent with partial covering. In the next section we discuss the necessity of including partial covered fractions for fitting and interpreting the BAL system.

3.5. Partial Covered Fractions

In principle, given a fully-resolved absorption multiplet, one can uniquely determine both the optical depth and covered fraction as a function of velocity (Hamann *et al.* 1997). However, given that the quality of the data does not permit such a detailed analysis, we proceed under the assumption that the covered fraction is a constant function of velocity, but may vary from ion to ion. Allowing the covered fraction to vary, we re-fit the doublets of O VI, Ne VIII, Mg X and Si XII. Figure 5 shows the absorption profiles and best-fit flat profiles of these ions with a partial covered fraction after the removal of the narrow lines and the known Ly β in O VI. The fits for the strongly-blended doublets of the other identified lithium-like ions C IV and N V are also shown for completeness, assuming a covered fraction of unity. The best fit of the higher-order Lyman lines, showing only the contributions from the continuum and broad absorption features, is plotted in Figure 6. We not only fit the resolved features Ly γ through Ly ϵ but also included lines through Ly29 to fit the spectrum down to the BAL Lyman limit. Around 2980 Å the continuum flux begins to be depressed significantly beyond the 20% level, presumably due to the high-order Lyman-line and Lyman-limit absorption from the $z = 2.246$ narrow-line system.

The resulting best-fit values for the covered fractions are listed in Table 5, along with minimum covered fractions for the singlet features derived from the penetration depths of the troughs. As is evident from comparing the values derived from the different absorption profiles, the uncertainty in constraining the covered fractions due to the choice of absorption profile is larger in most cases than that derived from the statistics of the fits. In Figure 7 we plot the covered fractions from the flat profile fits against the creation ionization potential for each ion. The closed circles are best-fit values derived from multiple components, while the open circles represent lower limits. It is possible that many or most of the singlet absorption features are saturated. If this is the case, then the open circles in Figure 7 closely represent the true covered fractions and not just lower limits.

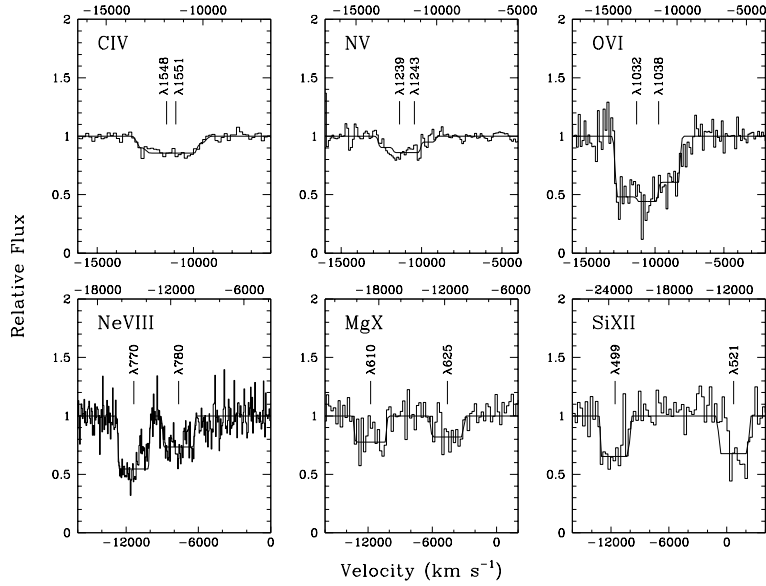


Fig. 5.— Absorption profiles of observed doublets from lithium-like ions along with the best-fit flat profiles. The identified narrow lines and the known $\text{Ly}\beta$ in O VI have been removed. The fits for the strongly-blended doublets of C IV and N V assume a covered fraction of unity, while the other fits allow for a partial covered fraction. The spectra are plotted as flux relative to the best-fit continuum against velocity relative to the wavelength of the blue (bottom axis) and red (top axis) components of the doublet in the QSO rest frame. For display purposes, the FOS G190H spectrum, which includes Mg X and Si XII, is rebinned by four pixels for higher S/N.

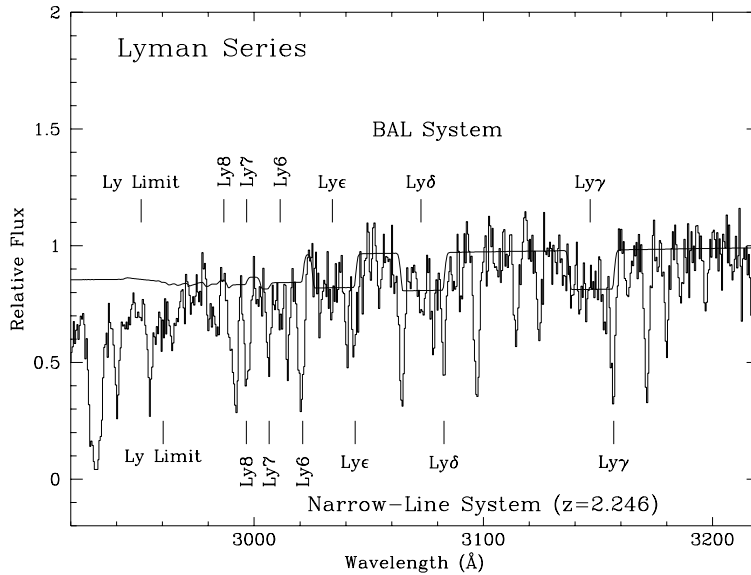


Fig. 6.— Best fit of the broad Lyman-series absorption lines of order $\text{Ly}\gamma$ and higher, plotted as flux relative to the best-fit continuum. To emphasize the broad lines the contribution of the narrow lines to the fit are not shown. Around 2980 \AA the depression of the continuum flux due to the $z = 2.246$ narrow-line system becomes significant. The location of the Lyman limit and Lyman series lines from this narrow-line system are indicated. The narrow lines of order $\text{Ly}6$ and higher are strongly blended with other lines.

Table 4. Minimum Column Densities

Ion	Flat Profile $\log N_j(\text{cm}^{-2})$	Gaussian $\log N_j(\text{cm}^{-2})$
H I ^a	14.84 ± 0.03	14.89 ± 0.05
C IV	14.64 ± 0.04	14.77 ± 0.06
N V	14.74 ± 0.04	14.84 ± 0.04
O VI	15.77 ± 0.04	15.79 ± 0.04
Ne V	15.91 ± 0.08	15.89 ± 0.14
Ne VI	15.83 ± 0.08	...
Ne VII	15.51 ± 0.08	15.39 ± 0.14
Ne VIII	15.90 ± 0.02	15.98 ± 0.03
Mg X	15.87 ± 0.06	15.92 ± 0.10
Si XII	16.25 ± 0.06	16.34 ± 0.08
Ar VII	14.62 ± 0.08	14.70 ± 0.10

^aDerived from Ly α only

Table 5. Covered Fractions

Ion	Flat Profile c_f	Gaussian c_f
H I ^a	$> 0.27 \pm 0.02$	$> 0.34 \pm 0.02$
H I ^b	0.17 ± 0.01	0.16 ± 0.01
C IV	$> 0.14 \pm 0.01$	$> 0.18 \pm 0.02$
N V	$> 0.13 \pm 0.01$	$> 0.21 \pm 0.03$
O VI	0.57 ± 0.02	0.52 ± 0.01
Ne V	$> 0.31 \pm 0.05$	$> 0.35 \pm 0.07$
Ne VI	$> 0.41 \pm 0.05$...
Ne VII	$> 0.38 \pm 0.05$	$> 0.40 \pm 0.07$
Ne VIII	$0.75^{+0.25}_{-0.05}$	$0.81^{+0.19}_{-0.10}$
Mg X	$0.24^{+0.09}_{-0.05}$	0.22 ± 0.03
Si XII	0.35 ± 0.04	0.38 ± 0.03
Ar VII	$> 0.22 \pm 0.04$	$> 0.28 \pm 0.02$

^aDerived from Ly α only

^bDerived from Lyman-series lines of order Ly γ and higher

Blending of the observed BALs with weak broad lines or with narrow lines could be important in the determination of the covered fractions because a fairly small change in the profile of one of the components of a doublet could cause a significant change in the inferred covered fraction. As mentioned previously, it appears that such contamination does exist in the Si XII and Mg X doublets, and it is likely that this is true to some extent for the O VI and Ne VIII features as well. Hence the true uncertainties in the covered fractions for these ions are probably somewhat larger than the listed statistical errors. This is not so much the case for H I, for which the covered fraction is determined from several lines and is therefore more reliable.

Despite this complication, it is clear that the covered fraction for the dominant absorbing source is not the same for all ions. The most convincing evidence for this is provided by the higher-order Lyman lines, for which we can reliably constrain the covered fraction to be less than 0.2. This covered fraction is less than that of most of the other lines, including the doublets of O VI, Ne VIII, and Si XII, as well as the observed singlet features, all of which depress the flux more than 20%. Therefore there must be multiple absorbing regions contributing to the BAL system, providing direct evidence for inhomogeneity in the ionization structure of the BAL gas. There appears to be a general trend for the very high-ionization species (creation IP \gtrsim 100 eV) to occult more of the continuum source than the lower-ionization species (creation IP \lesssim 100 eV).

Since we can constrain well the covered fraction of H I, it is useful to estimate a better lower limit on the column density of H I, as this provides a very useful constraint for our photoionization models (§4). For the fit of the Lyman lines with a partial covered fraction, a large column density of H I, $\log N(H) > 17$, is required to obtain a good fit. However, as mentioned previously, there is probably some narrow-line blending, which could cause us to slightly overestimate the strength of the higher-order Lyman lines. To get a more conservative lower limit on the column density of H I, we allowed for the contribution of additional narrow lines below the 3σ significance level that appear to be blended with the broad lines. With these lines included, we find that with 90% confidence a column density of $\log N(H) \gtrsim 16.87$ is necessary to provide a good fit using a flat profile, and $\log N(H) \gtrsim 16.83$ using a Gaussian profile. An important point is that we can make these estimates because we can clearly see the higher-order Lyman lines usually not visible in BAL spectra. The fact that the Ly α feature indicates a larger covered fraction than the higher-order Lyman lines suggests that there are at least two different regions causing absorption in H I – a region with a small covered fraction but a high column density of H I that contributes the absorption for the higher-order Lyman lines, and a region with a lower column density of H I but significantly higher covered fraction that dominates the observed Ly α absorption profile. As a result, if we were to estimate the total column of H I in this BAL system from Ly α alone and assume a covered fraction of unity, we would underestimate the true value by orders of magnitude.

4. DISCUSSION

4.1. Photoionization Models

In order to produce self-consistent photoionization models we construct an ionizing continuum based on the observed continuum. However, to accurately represent the EUV continuum, particularly for a high-redshift QSO, we need to first correct for the accumulated Lyman-line and Lyman-continuum absorption from intervening clouds, the primary characteristic of which is a broad trough centered around 700 Å known as the Lyman valley (Møller & Jakobsen 1990). We use the empirical formula for the statistics of the forest-line distribution

$$\frac{\partial^2}{\partial z \partial N} = A(1+z)^\gamma N^{-\beta} \quad (1)$$

(Press & Rybicki 1993). For the parameter values we adopt $\beta = 1.5$, $A = 2.4 \times 10^7$, and $\gamma = 2.46$, since these yield a line number in agreement with observations of high-redshift QSOs (Hu *et al.* 1995). Using this distribution we applied the statistical correction for $z = 2.361$, including intervening absorbers with a total column density between 10^{13} cm^{-2} and 10^{16} cm^{-2} . Any absorption system with a column density greater than $\sim 10^{16} \text{ cm}^{-2}$ produces a significant Lyman limit feature for which we can correct directly, which we did for the $z = 0.721$ and $z = 2.246$ systems. The resulting corrected spectrum is plotted in Figure 8, shifted into the QSO rest frame. Also shown for comparison, with arbitrary normalization, is the composite spectrum of radio-quiet QSOs produced by Zheng *et al.* (1997). The lines below the spectrum indicate the wavelength regions used to fit the continuum of SBS1542+541. The spectrum shows a break in the power-law index α ($L_\nu \propto \nu^\alpha$) around 1000 Å. Such a break is consistent with Zheng *et al.* (1997), who find that a break in the UV power-law index around 1050 Å is a general feature of QSO continua. From the Steward spectrum we derive a near-UV power-law index of $\alpha_{NUV} = -0.64 \pm 0.02$ by fitting the region 1700 – 2240 Å, longward of the break. Shortward of the break, we use the FOS data to derive an extreme-UV power-law index of $\alpha_{EUV} = -1.59 \pm 0.03$ by fitting the continuum range 360 – 960 Å.

To estimate the soft X-ray flux from the *ROSAT* PSPC data, we use the total count rate of $7.02 \times 10^{-3} \text{ count s}^{-1}$ in the observed energy band 0.1 – 2.5 keV (0.3 – 8.4 keV in the rest frame) and the Galactic neutral hydrogen column density of $N(H) = 1.30 \times 10^{20} \text{ cm}^{-2}$. Assuming a power-law index of $\alpha_x = -1.7$, a typical value for the soft X-ray (~ 0.1 – a few keV) continuum of radio-quiet QSOs as derived from PSPC observations (Schartel *et al.* 1995; Laor *et al.* 1997), the observed flux at 1 keV is $5.7 \times 10^{-32} \text{ erg cm}^{-2} \text{ s}^{-1} \text{ Hz}^{-1}$, which corresponds to a flux of $1.3 \times 10^{-31} \text{ erg cm}^{-2} \text{ s}^{-1} \text{ Hz}^{-1}$ at 1 keV in the QSO rest frame. This is an order of magnitude less flux than expected based on an extrapolation of the extreme-UV continuum. We illustrate this in Figure 9 by plotting the extrapolated extreme-UV continuum and the derived X-ray continuum. We also show the continuum derived from the *ROSAT* data assuming $\alpha_x = -1.0$, a more typical value for harder X-rays (\gtrsim a few keV; Comastri *et al.* 1992; Williams *et al.* 1992).

The relative luminosity between the optical and the X-ray is commonly represented by the parameter $\alpha_{ox} = (\log F_o - \log F_x)/2.605$, where F_o is the spectral flux at 2500 Å and F_x is the

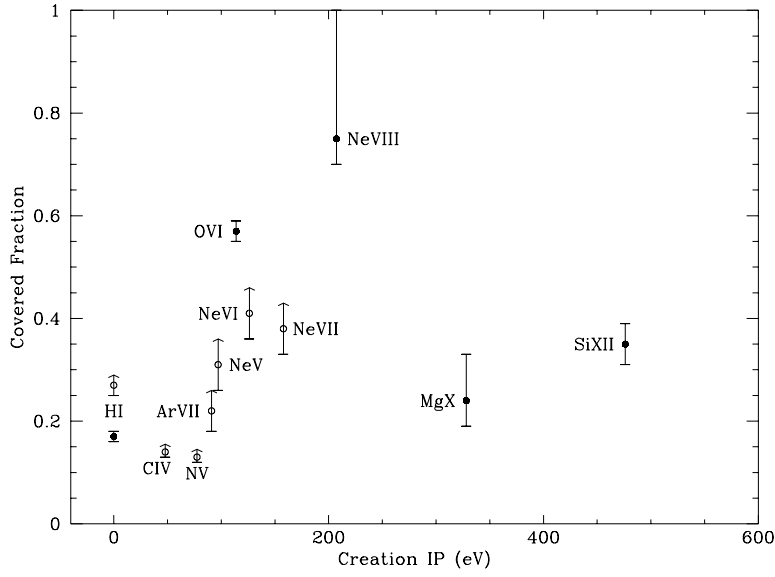


Fig. 7.— Covered fractions and creation IPs of various ions derived from the flat profile fits. The closed circles are best-fit values derived from multiple components, while the open circles represent lower limits based on the penetration depths of the troughs. The errors, particularly on the best-fit values, could be significantly larger if the observed BALS are blended with other features. However, the best-fit covered fraction of H I is fairly reliable since it is determined from several lines. Two values are plotted for H I, the minimum value derived from Ly α only and the best-fit value based on the higher-order Lyman lines.

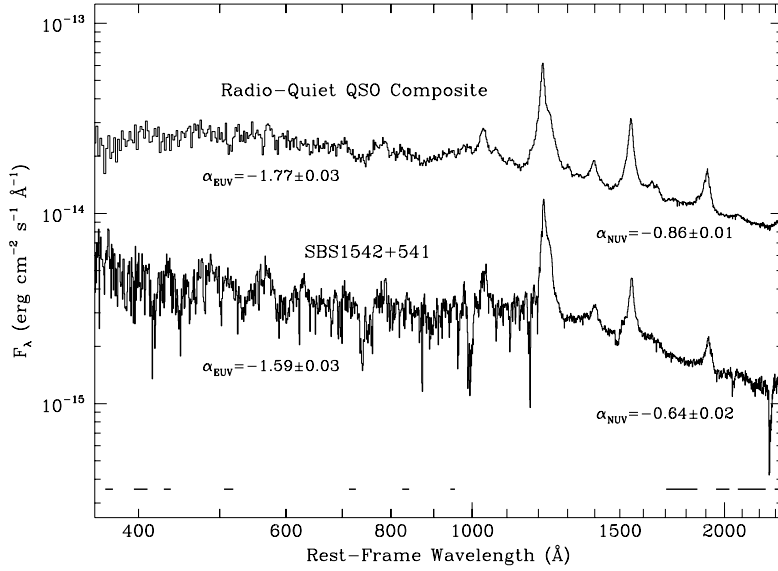


Fig. 8.— Combined spectra, corrected for intervening absorption, shown with the radio-quiet QSO composite of Zheng *et al.* (1997) for comparison. The composite has been arbitrarily normalized. The lines below the spectra indicate the wavelength regions used to fit the continuum of SBS1542+541. This continuum exhibits a break in the power-law index around 1000 \AA , similar to the composite spectrum.

flux at 2 keV. An extrapolation of the near-UV continuum yields a rest-frame flux at 2500 Å of $F_o = 2.8 \times 10^{-27}$ erg cm⁻² s⁻¹ Hz⁻¹, and from the X-ray data we infer a rest-frame flux at 2 keV of $F_x = 4.0 \times 10^{-32}$ erg cm⁻² s⁻¹ Hz⁻¹, yielding $\alpha_{ox} = 1.86$. Such a high value for α_{ox} is consistent with the results of Green & Mathur (1996), who find values of $\alpha_{ox} \gtrsim 1.8$ in a sample of BALQSOs observed with the *ROSAT* PSPC. The authors attribute the lack of X-ray flux to absorption by the BAL gas and derive BAL column densities $\gtrsim 2 \times 10^{22}$ cm⁻². It is therefore reasonable to suspect that the X-ray continuum of SBS1542+541 may be absorbed by the BAL gas. Hence, to choose an intrinsic ionizing continuum for our photoionization models, we defer to the UV observations and use the extrapolated power law with index $\alpha = -1.59$ shown in Figure 9. The possibility of X-ray absorption is further discussed in §4.2. In §4.3 we discuss the effect of choosing an alternative continuum shape.

All of our calculations were performed with the photoionization code CLOUDY (version 90.01; Ferland 1996). We assume that the BAL gas is in photoionization equilibrium with the intrinsic QSO continuum and has solar chemical abundances. We use a constant density of $n_H = 10^8$ cm⁻³, although it has been previously established (*e.g.* Hamann *et al.* 1995) in similar models that the ionization state of the gas is not sensitive to the absolute density (up to a limit of $\sim 10^{11} - 10^{12}$ cm⁻³). Hence our results are valid for any reasonable space density, so long as it is constant. The continuum normalization is determined by the ionization parameter U , defined as the ratio of the number density of ionizing photons (energy above the ionization threshold of hydrogen) to hydrogen nuclei,

$$U = \int_{\nu_{th}}^{\infty} \frac{F_\nu}{ch\nu n_H} d\nu, \quad (2)$$

where ν_{th} is the frequency at the hydrogen ionization threshold. We do not assume that the gas is optically thin to the ionizing continuum. In fact, given the necessarily large total column densities that we infer, continuum opacity must be an important factor and will alter the spectral energy distribution of the ionizing continuum as it propagates through the BAL gas, resulting in changes in the ionization state.

4.1.1. Single-Slab Model

The simplest model of the BAL gas is a single slab characterized by its total column density N_H and the ionization parameter U at the face of the slab. We use our measured limits on the ionic column densities to constrain the total column density and ionization parameter for such a model. We illustrate this in Figure 10 by plotting in the $N_H - U$ parameter space contours of constant ionic column density equal to a few of our lower limits, including those which provide the most restrictive constraints on the parameters. The contour for H I corresponds to a column density of $10^{16.8}$ cm⁻². Models consistent with our lower limits on the column densities must lie above the solid lines. We also include a constraint from the lack of Si IV absorption. By fitting the data assuming a flat absorption profile with a centroid at -11400 km s⁻¹, a width of 2000

km s⁻¹, and a covered fraction of 0.2, we derive an upper limit on the column density of Si IV of 10^{14.1} cm⁻² with 90% confidence. This upper limit is represented by the dashed line in Figure 10. Models consistent with the upper limit must lie below the dashed line to avoid producing an observable amount of Si IV. Thus the shading indicates the region of parameter space consistent with our column density limits in this simple model.

The existence of a region in the $N_H - U$ parameter space that satisfies all of our column density constraints means that, based on the column density limits alone, we could explain the observations by a model of a single, marginally optically thick, BAL region of constant density. In such a model the large range of ionization states is possible because the very high-ionization states would exist near the face of the slab, whereas the lower-ionization states exist deeper in the slab (*i.e.* farther from the continuum source) as a result of X-ray self-shielding. However, to understand the BAL system we would like to be able to explain not only the ionization state of the gas but also the covered fractions, and in particular the correlation of a higher covered fraction with a higher state of ionization. This would be impossible to achieve in a single-zone model. We now discuss how we can modify this simple single-slab picture to arrive at a more plausible explanation of the covered fractions.

4.1.2. Two-Slab Model

Multiple zones are necessary to explain the range in covered fractions that we observe. Empirically, what is required is that the high-ionization gas have a larger covered fraction than the lower-ionization gas. Here we divide the BAL region into two zones, one with a low covered fraction contributing the absorption from the higher-order Lyman lines and perhaps also C IV and N V, and another with a higher covered fraction providing the dominant absorption source of the higher-ionization species, up through Si XII. We will refer to these as the “smaller” and “larger” zones, respectively. Figure 11 shows the constraints for each zone provided by our observed column density limits as in the single-slab case. For the larger zone we apply an additional constraint provided by the fact that N V absorption clearly cannot be optically thick in this zone. In the same manner as described in the previous section for Si IV, but here assuming a covered fraction of 0.4, we place an upper limit of 10^{15.2} cm⁻² on the column density of N V. Placing upper limits on the column densities of C IV and O V results in constraints that are very similar but slightly less-restrictive, so they are not shown.

Further plausible physical assumptions can place more restrictions on the possible range of parameter space covered by the two zones. For example, we could assume that the clouds that make up the BAL gas are equidistant from the central radiation source, but have small, dense cores surrounded by lower-density halos. The cores would naturally have a lower ionization parameter, and they would cover a smaller fraction of the source. More generally, one could envision a density-fluctuated medium containing small, dense clouds of radius R_s , and larger, lower-density clouds of radius R_l satisfying the constraint $R_s < R_l$, where we use the subscripts s

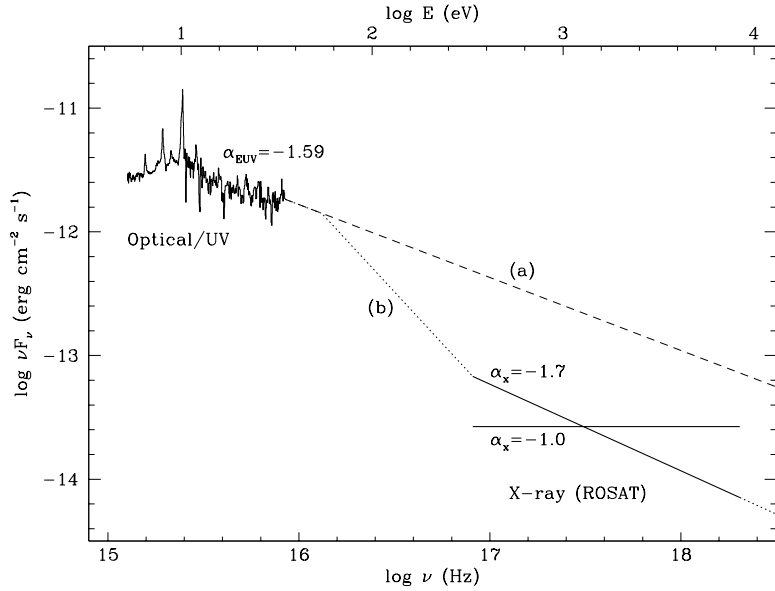


Fig. 9.— Broad-band continuum of SBS1542+541, including the optical/UV spectra and the X-ray continuum as normalized by *ROSAT* data. The two lines for the X-ray continuum correspond to different assumptions for the X-ray spectral index, $\alpha_x = -1.7$ and $\alpha_x = -1.0$. The dashed and dotted lines, (a) and (b), illustrate different models considered for the ionizing continuum. Model (a) is an extrapolation of the EUV continuum throughout the X-ray band. Model (b) connects the EUV continuum to the *ROSAT* data by introducing a break at the location of the He II ionization edge (54 eV).

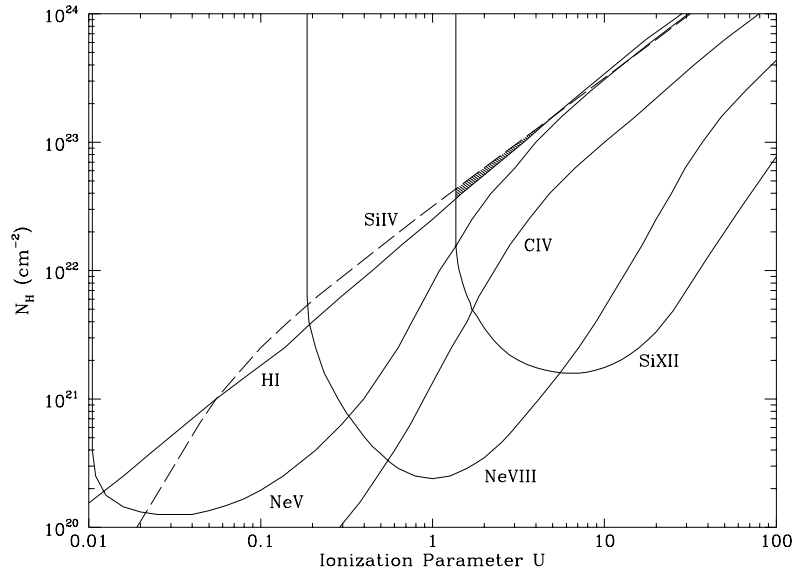


Fig. 10.— Constraints on the total column density and ionization parameter for a single-slab model. The solid lines are contours of constant ionic column density corresponding to our measured lower limits, while the dashed line represents an upper limit. A particular choice of parameters must lie in the parameter space above the solid lines and below the dashed line to produce a model consistent with the column density limits. The shaded region satisfies all of these constraints.

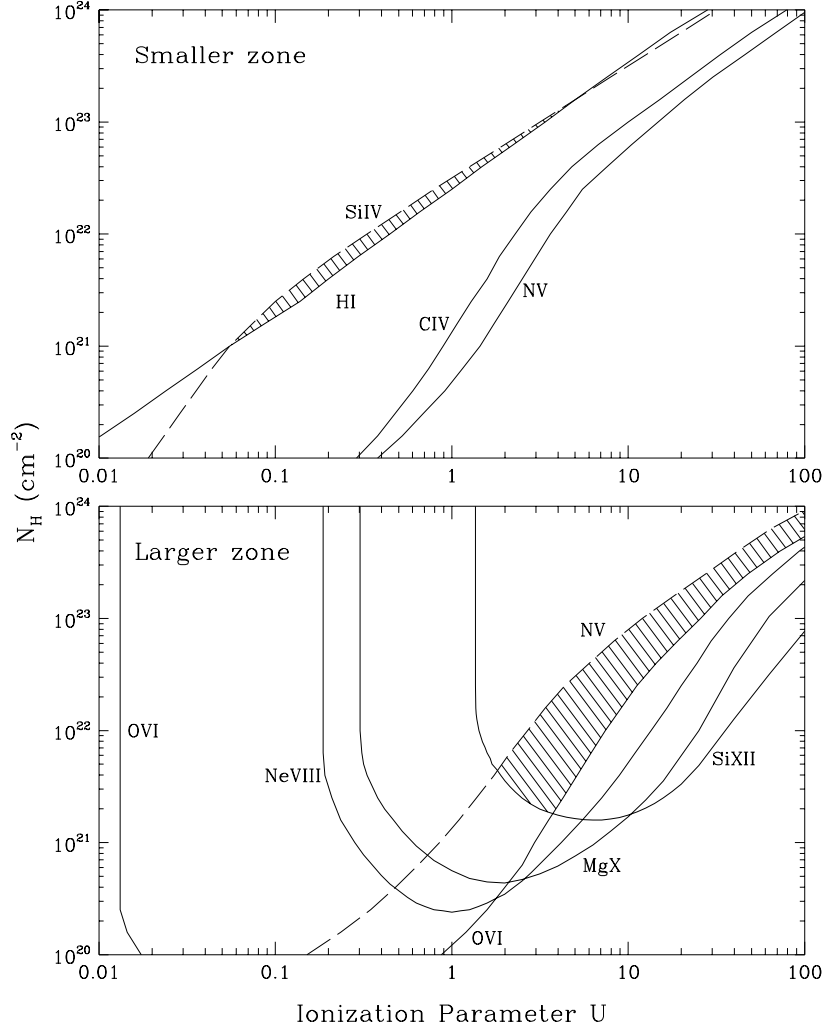


Fig. 11.— Constraints on the total column density and ionization parameter for a two-slab model. The system is separated into a larger zone and a smaller zone based on the observed covered fractions. The solid lines indicate lower limits on the ionic column densities, the dashed lines indicate upper limits, and the shaded regions satisfy the column density constraints applied to each zone.

and l to denote the smaller and larger zones, respectively. We can relate the cloud radii to their column densities as $R \propto N_H/n_H$. Since $U \propto 1/(r^2 n_H)$, we have $R \propto r^2 N_H U$. Assuming the two zones are at roughly the same distance r from the continuum source, we can therefore write the size constraint as $N_{H,s} U_s < N_{H,l} U_l$. This reduces the range of acceptable two-slab models in the four-dimensional parameter space spanned by U_s , $N_{H,s}$, U_l , and $N_{H,l}$. By considering the effect of this constraint on the solutions shown in Figure 11, we conclude that, in this density fluctuation model, the ionization parameter in the smaller zone must be a factor $\gtrsim 2$ lower than in the larger zone, which would correspond to a larger density in the smaller zone by the same factor.

Density fluctuations in the BAL gas and the resulting correlation between covered fraction and ionization state could have implications for the determination of chemical abundances in BAL systems. Studies of BAL systems typically find that a large range in ionization parameters (more than an order of magnitude) and large abundance modifications relative to solar (as much as an order of magnitude, or even two for nitrogen) are necessary to explain the observed column densities (*e.g.* Turnshek *et al.* 1996). The large metallicity enhancements are required primarily because of the observed weakness of the Ly α BAL, which is used to derive the H I column density. However, in the BAL system of SBS1542+541, the small equivalent width of Ly α despite a large optical depth ($\tau_{\text{Ly}\alpha} > 50$) is explained by the fact that most of the H I covers only a small fraction of the continuum source. As a result, the contribution from most of the H I is “hidden” beneath the absorption from more highly-ionized gas with a much lower column density but higher covered fraction. This situation is revealed by the direct observation of the saturated Lyman lines of order Ly γ and higher, lines that in a more typical BAL system would not be visible due to blending with other lines, particularly C III $\lambda 977$. If inhomogeneity of the BAL gas is a generic feature of BAL systems, particularly that which would result in large columns of hidden H I, then this could affect (and make more difficult) the measurement and interpretation of BAL column densities and chemical abundances.

In this model, the source of the H I absorption is constrained to the small region of parameter space shown in Figure 11 by the tight upper limit on Si IV absorption. However, it is possible that the H I absorption arises in a very weakly-ionized zone ($U \lesssim 10^{-4}$) with a low enough column density ($N_H \lesssim 10^{18} - 10^{19} \text{ cm}^{-2}$) that no strong low-ionization metal absorption lines are produced. If such a zone exists, then the C IV and N V lines require an additional higher-ionization zone. This arrangement is illustrated in Figure 12, as calculated using continuum shape (b) from Figure 9 (see §4.3). Alternatively, they could be produced in the larger zone if the lines are assumed to be not optically thick. This is unlikely, however, since the profiles, particularly C IV, strongly suggest saturation.

Although a two-zone model is the simplest one that can explain the basic properties of the system, including the observed line strengths and the general trend of the covered fractions, there are complications. In particular, the observed range in covered fractions for the highly-ionized species, especially the apparently high covered fraction of Ne VIII, cannot be explained by a simple model. If this is a real effect, then the physical structure of the BAL gas could be extremely

complex, and much more detailed modeling would be necessary to reproduce this peculiar behavior. However, it is entirely possible that this effect is simply due to the uncertainties induced by blending and the choice of fitting profile.

4.1.3. Disk-Like Geometry

The correlation of covered fraction with ionization state can also be explained by more complex physical models. It is plausible that the BAL region has an overall disk-like geometry as suggested by the high continuum and even higher trough polarization observed in BALQSOs (Goodrich & Miller 1995; Cohen *et al.* 1995). This has been explored theoretically in the disk-wind models of AGN broad line regions (Murray *et al.* 1995; Murray & Chiang 1995). One can imagine that we are looking along a particular line of sight, just above (or below) the disk, as illustrated schematically in Figure 13. The states of lower ionization, being farther from the continuum source, would naturally have a smaller covered fraction. An appealing consequence of this interpretation is that the BAL region that we observe in SBS1542+541 would not be required to be inherently exceptional in its lack of absorption from states of lower ionization such as Si IV, O IV, and C III. These ions could be part of the BAL region but be far enough from the continuum source that they lie outside our line of sight.

4.2. Possible X-Ray Absorption

The existence of high column densities of highly-ionized gas suggests that the UV absorption system of SBS1542+541 is associated with a “warm absorber” as seen in the X-ray spectra of many low-redshift AGN. Models of X-ray warm absorbers (Netzer 1993; Krolik & Kriss 1995; Netzer 1997) predict that the strongest features should be the K ionization edges of O VII and O VIII as well as K and L edges of ionization stages of iron \sim Fe XX. According to our photoionization calculations, given the likely range of ionization parameters for the BAL gas in SBS1542+541, the dominant stages of oxygen should be O VII and O VIII. The predicted large column densities of these ions should produce observable ionization edges at 0.22 keV (O VII) and 0.26 keV (O VIII), each with an optical depth of $\tau > 0.2$. Observations of these X-ray features would enable us to form a much more complete picture of the ionization state of the system, making this object a good candidate for further study of the unification of X-ray/UV absorbers (Mathur *et al.* 1994; Mathur, Elvis, & Wilkes 1995; Mathur, Wilkes, & Aldcroft 1997).

4.3. Continuum Shape

We now consider the possibility that the weak X-ray flux is an intrinsic characteristic of the continuum being intercepted by the BAL region; *i.e.* it is not due primarily to X-ray absorption by

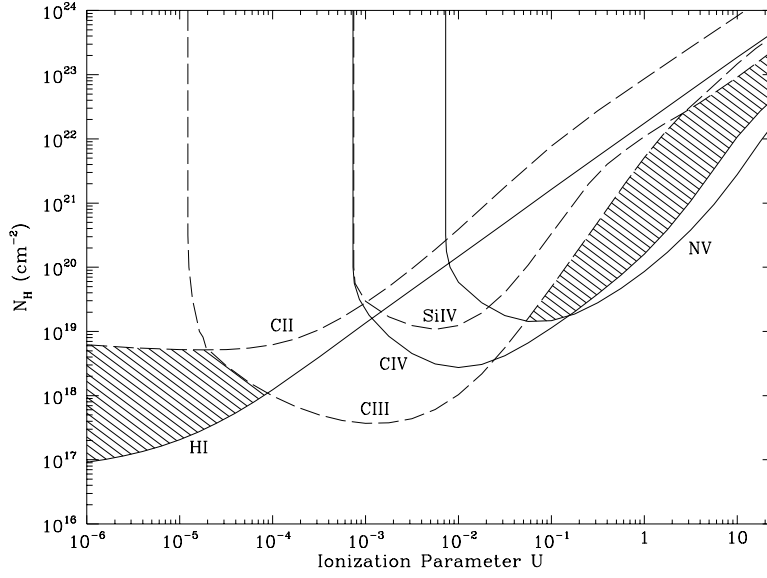


Fig. 12.— Some contours of constraint for the ions with a small covered fraction as shown in the top of Figure 11 but now produced using continuum shape (b) from Figure 9. At least two zones, represented by the shaded regions, are necessary to explain the observations: a low column density, weakly-ionized zone (left) producing the H I absorption and a more highly-ionized, larger column density zone (right) producing the C IV and N V absorption. Upper limits on some low-ionization species constrain the zones.

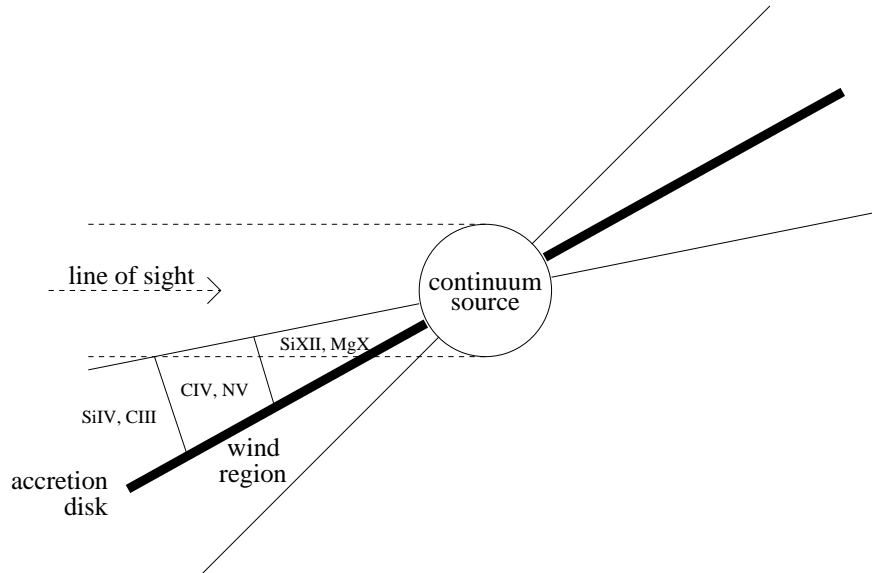


Fig. 13.— Schematic illustration of a disk-like BAL geometry as viewed from a line of sight just above the disk. Because of the geometry, the more weakly-ionized gas, which lies farther away from the continuum source, will cover less of the source along such a line of sight. A typical BAL sight line would be directly into the disk wind.

the BAL gas itself. For this purpose we have repeated our photoionization calculations using the ionizing continuum shape labeled (b) in Figure 9. Here we connect the X-ray continuum inferred from the *ROSAT* flux assuming $\alpha_x = -1.7$ with the EUV continuum by arbitrarily introducing a break in the EUV power-law index at the location of the He II ionization edge (54 eV). The break point is chosen to be consistent with the UV observations (below our wavelength coverage), but at a low enough energy that it should maximize the effects on the results.

Naturally, due to the softer continuum, much higher ionization parameters are necessary to produce the highest observed ionization states, $U > 10$ for Si XII. More interestingly, the contours of constraint from H I and Si IV shift relative to one another such that the solution for the smaller zone shown in Figure 11 does not exist for this model. That is, one cannot construct a simple model of the smaller zone that produces the necessary columns of H I, C IV, and N V that does not also produce a large column density of Si IV. The only explanation in this model for the H I absorption, therefore, is that there is a very weakly-ionized, low column density zone as mentioned in §4.1.2. Figure 12 shows the location of such a zone in the $N_H - U$ parameter space, using upper limits of $10^{15.2} \text{ cm}^{-2}$ on C II (from $\lambda 1335$) and $10^{14.0} \text{ cm}^{-2}$ on C III (from $\lambda 977$), again derived in the same manner as for Si IV. This would require an enormous spread in ionization parameters (5 orders of magnitude) between the different zones. Since the existence of a zone with such a different ionization state, yet having a very similar distribution in velocity space, is not particularly appealing, this indirectly suggests that the ionizing continuum extrapolated from the EUV (labeled (a) in Figure 9) is a better representation of the true continuum and that the weak X-ray flux is indeed a consequence of X-ray absorption.

5. SUMMARY

The BAL system of SBS1542+541 has several unusual properties. The most interesting are:

1. The state of ionization is extremely high, higher than what is typically inferred for “classical” BAL systems from the study of the UV absorption lines. Strong absorption is present from the highly-ionized lithium-like ions of O VI, Ne VIII, Mg X and even Si XII, which has a creation ionization potential of 476 eV. Absorption from Si IV, nearly always present in BAL spectra, is undetected. It should be noted that high ionization similar to this has been suggested in connection with BALs, but this is based on X-ray rather than UV absorption properties (Mathur, Elvis, & Singh 1995). The high state of ionization and large column density ($> 2 \times 10^{21} \text{ cm}^{-2}$) suggest that the BAL system should be associated with an X-ray “warm absorber”.
2. The covered fractions for the various absorbing ions are in at least some cases significantly less than unity. Even more interesting is that the covered fraction is apparently ion-dependent with a general trend towards higher covered fractions with higher states of ionization. This could be caused by either a special line of sight through a BAL disk or by the existence of

multiple ionization zones in the BAL gas, possibly as a result of density fluctuations.

These properties make the BAL system of SBS1542+541 observationally unique and certainly intriguing. It begs the question—is this system extraordinary, or is it telling us something important about the character of BALQSOs in general? The weakness of the standard BALs of $\text{Ly}\alpha$, C IV, N V, and Si IV is clearly unusual compared to “classical” BALQSOs. However, the lack of observed Si IV and other low-ionization species itself is perhaps not so surprising given the weakness of C IV, particularly if complex covered-fraction effects are involved. The very high-ionization species we observe in SBS1542+541 occur in the rest-frame EUV, a spectral region not usually observable due to intervening Lyman-limit absorbers. Hence the existence of these ions is not inconsistent with other BALQSOs, for which it is not possible to confirm or deny their presence. It therefore seems plausible that the ionization state of this system is similar to that of normal BALQSOs. If the existence of large column densities of very highly-ionized gas and/or non-trivial ionization structure as we find in SBS1542+541 are common properties of BAL systems, then this object could indeed be providing important clues to the nature of the BAL phenomenon.

This work is based on observations with the NASA/ESA Hubble Space Telescope, obtained at the Space Telescope Science Institute, which is operated by the Association of Universities for Research in Astronomy, Inc., under NASA contract NAS5-26555. Support for this research was provided by NASA grant NAG5-1630 for the Faint Object Spectrograph team, and NASA contract NAS5-27000 for the Hopkins Ultraviolet Telescope.

REFERENCES

- Barlow, T. A., & Junkkarinen, V. T. 1994, BAAS, 25, 1339
- Boroson, T. A., & Meyers, K. A. 1992, ApJ, 397, 442
- Cardelli, J. A., Clayton, G. C., & Mathis, J. S. 1989, ApJ, 345, 245
- Cohen, M. H. *et al.* 1995, ApJ, 448, 77
- Comastri, A. *et al.* 1992, ApJ, 384, 62
- Davidson, A. F., Kriss, G. A., & Zheng, W. 1996, Nature, 380, 47
- Ferland, G. J. 1996, “HAZY a Brief Introduction to Cloudy,” Univ. Kentucky, Dept. Physics & Astron., Internal Rep.
- Goodrich, R. W., & Miller, J. S. 1995, ApJ, 448, 73
- Green, P. J., & Mathur, S. 1996, ApJ, 462, 637
- Hamann, F. *et al.* 1995, ApJ, 443, 606
- Hamann, F., Barlow, T. B., & Junkkarinen, V. 1997, ApJ, 478, 87
- Hamann, F., Barlow, T. B., Junkkarinen, V., & Burbidge, E. M. 1997, ApJ, 478, 80
- Hamann, F., Korista, K. T., & Morris, S. L. 1993, ApJ, 415, 541
- Hu, E. M., Kim, T.-S., Cowie, L. L., Songaila, A., & Rauch, M. 1995, AJ, 110, 1526
- Korista, K. T. *et al.* 1992, ApJ, 401, 529
- Korista, K. T., & Arav, N. 1997, in ASP Conf. Ser. 128, Mass Ejection from AGN, ed. N. Arav, I. Shlosman, & R. J. Weymann (San Francisco: ASP), 201
- Kriss, G. A. 1994, in ASP Conf. Ser. 61, Astronomical Data Analysis Software and Systems III, ed. D. R. Crabtree, R. J. Hanisch, & J. Barnes (San Francisco: ASP), 437
- Krolik, J. H., & Kriss, G. A. 1995, ApJ, 447, 512
- Laor, A., Fiore, F., Elvis, M., Wilkes, B. J., & McDowell, J. C. 1997, ApJ, 477, 93
- Mathur, S., Elvis, M., & Singh, K. P. 1995, ApJ, 455, 9
- Mathur, S., Elvis, M., & Wilkes, B. 1995, ApJ, 452, 230
- Mathur, S., Wilkes, B. J., & Aldcroft, T. 1997, ApJ, 478, 182
- Mathur, S., Wilkes, B., Elvis, M., & Fiore, F. 1994, ApJ, 434, 493
- Møller, P., & Jakobsen, P. 1990, A&A. 228, 299
- Murray, N., Chiang, J., Grossman, S. A., & Voit, G. M. 1995, ApJ, 451, 498
- Murray, N., & Chiang, J. 1995, ApJ, 454, 105
- Netzer, H. 1993, ApJ, 411, 594
- Netzer, H. 1997, ApJ, 473, 781

- Press, W. H., & Rybicki, G. B. 1993, *ApJ*, 418, 585
- Schartel, N. *et al.* 1996, *MNRAS*, 283, 1015
- Shull, J. M., & Van Steenberg, M. E. 1985, *ApJ*, 294, 599
- Stark, A. A. *et al.* 1992, *ApJS*, 79, 77
- Turnshek, D. A. 1984, *ApJ*, 280, 51
- Turnshek, D. A. 1988, in *QSO Absorption Lines: Probing the Universe*, ed. S. C. Blades, C. A. Norman, & D. A. Turnshek (Cambridge: Cambridge Univ. Press), 17
- Turnshek, D. A., Monier, E. M., Sirola, C. J., & Espey, B. R., 1997, *ApJ*, 476, 40
- Turnshek, D. A. *et al.* 1996, *ApJ*, 463, 110
- Verner, D. A., Barthel, P. D., & Tytler, D. 1994, *A&A*, 108, 287
- Vogel, S. & Reimers, D. 1995, *A&A*, 294, 377
- Weymann, R. J., Carswell, R. F., & Smith, M. G. 1981, *ARA&A*, 19, 41
- Williams, O. R. *et al.* 1992, *ApJ*, 389, 157
- Zheng, W., Kriss, G. A., Telfer, R. C., Grimes, J. P., & Davidsen, A. F. 1997, *ApJ*, 475, 469